UDK 620.17:539.374:669.721.5
Original scientific article/Izvirni znanstveni članek

ISSN 1580-2949
MTAEC9, 55(6)781(2021)

HOT DEFORMATION BEHAVIOR AND PROCESSING MAP OF A Mg-Gd-Y-Zn-Zr ALLOY

OBNAŠANJE ZLITINE Mg-Gd-Y-Zn-Zr MED VROČO DEFORMACIJO IN NJENA PROCESNA MAPA

Zhaoming Yan[1*], Jiaxuan Zhu[2], Zhimin Zhang[1,2], Qiang Wang[1], Yong Xue[1]

[1]School of Materials Science and Engineering, North University of China, Xueyuan Road, Taiyuan, China
[2]College of Mechatronics Engineering, North University of China, Xueyuan Road, Taiyuan, China

Prejem rokopisa – received: 2021-06-06; sprejem za objavo – accepted for publication: 2021-09-30

doi:10.17222/mit.2021.212

Compression tests of a Mg-13Gd-4Y-2Zn-0.5Zr alloy were carried out on a Gleeble-1500D thermo-mechanical simulator within a temperature range of 420–500 °C and strain rate of 0.001–5 s^{-1} so that the corresponding flow behavior was investigated. The Zener-Hollomon parameter *Z* was used in a hyperbolic-sine-type equation to express the relationships between the peak stress, deformation temperature and strain rate. Work hardening, dynamic recovery and dynamic recrystallization were the main characteristics affecting the plastic-deformation behaviors. The activation energy *Q* was calculated to be 208.2 kJ/mol and processing maps at strains of 0.3, 0.5 and 0.7 were generated based on a dynamic material model. The optimum processing parameters were obtained with a power-dissipation analysis.

Keywords: Mg-Gd-Y-Zn-Zr alloy, hot-deformation behavior, processing maps, microstructure evolution

Povzetek: V članku je opisano izvajanje tlačnih preizkusov zlitine Mg-13Gd-4Y-2Zn-0,5Zr na termosimulatorju Gleeble-1500D v temperaturnem območju med 420 °C in 500 °C pri hitrostih deformacije od 0,001 s^{-1} do 5 s^{-1}. Avtorji so na osnovi tega raziskovali njeno plastično deformacijo. Uporabili so Zener-Hollomonov parameter *Z* v hiperboličnem tipu enačbe, ki izraža zvezo med vršno napetostjo, temperaturo in hitrostjo deformacije. Utrjevanje, dinamična poprava in rekristalizacija so glavne lastnosti, ki vplivajo na obnašanje materiala med njegovo plastično deformacijo. Izračunana je bila aktivacijska energija *Q* (208,2 kJ/mol), na osnovi dinamičnega materialnega modela pa so avtorji izdelali (generirali) deformacijske procesne mape izbrane zlitine pri deformacijah 0,3, 0,5 in 0,7. S pomočjo močnostne disipacijske analize so določili optimalne procesne parametre.

Ključne besede: zlitina Mg-Gd-Y-Zn-Zr, obnašanje med vročo deformacijo, procesne mape, razvoj mikrostrukture

1 INTRODUCTION

Magnesium (Mg) alloy, which is the lightest structural material used for industrial applications, has the advantages of a high specific strength/stiffness, good damping capacity and excellent electromagnetic shielding performance.[1–3] The development of rare-earth magnesium alloys has solved the problem of a low absolute strength, e.g., Mg-RE-Zn, which has a unique microstructure of long-period stacking-ordered (LPSO) structure.[4–6] However, poor ductility and hard-to-deform characteristics restrict their engineering applications owing to the hexagonal close-packed (HCP) crystal structure with limited slip systems. Elevating the deformation temperature, which can reduce the critical shear stress (CRSS) and induce a non-basal plane slip, can improve the plasticity of a Mg alloy.[7] Considerable research was carried out with various deformation methods, such as extrusion, forging and severe plastic deformation, to enhance the strength and ductility of these alloys to a great extent.[8–10] Homma et al.[8] studied mechanical behavior of Mg-1.8Gd-1.8Y-0.7Zn-0.2Zr prepared with hot extrusion at 400 °C and the ultimate tensile strength, tensile yield strength and fracture elongation were 542 MPa, 473 MPa and 8.0 %, respectively. Li et al.[11] investigated an ECAP-ed Mg-Gd-Y-Zn-Zr alloy, and the results showed that a fine-grained structure and a weakened texture were observed after a four-pass deformation, while the ultimate strength reached 361 MPa.

The thermomechanical process was mostly conducted on a Mg-RE-Zn alloy because of poor plasticity at room temperature. Hot processing highly depended on deformation parameters such as the temperature, strain and strain rate. Also, the dynamic recovery and recrystallization during deformation were closely related to these parameters.[12,13] Zhou et al.[14] studied the dynamic-recrystallization (DRX) behavior of the Mg-6.9Gd-3.2Y-1.5Zn-0.5Zr alloy after hot compression and proposed that a combination of the deformation temperature, strain rate and LPSO phase influenced the DRX ratio. Zhang et al.[15] investigated the microstructure evolution of the Mg-4Y-2Nd-0.2Zn-0.5Zr alloy, and the results showed that the DRX was influenced by deformation parameters and the precipitated particles facilitated continuous dynamic recrystallization (CDRX). In the present work, we aim to evaluate the parameters and mechanisms of hot deformation in the Mg-Gd-Y-Zn-Zr

*Corresponding author's e-mail:
zmyan1027@nuc.edu.cn (Z. Yan)

alloy with a view to understand the flow behavior and optimize its workability.

A processing map, which consists of a power-dissipation map and an instability map, can describe a hot-deformation process and establish the relationship between deformation parameters and the flow stress according to the dynamic-material model (DMM).[16,17] After the establishment and analysis of a processing map, we can adjust the microstructure of a Mg-Gd-Y-Zn-Zr alloy and improve its properties. According to the theory of DMM, a workpiece undergoing hot deformation is regarded as a nonlinear dissipater of power and the total dissipation P can be separated into two parts, i.e., the G content that is consumed by plastic deformation, most of which transforms into viscoplastic energy, while the rest is stored in crystal-distortion energy, and the J co-content that is consumed by microstructural evolution, such as dynamic recovery, DRX, phase transformation, etc. Thus, the instantaneous dissipated power is given as[18]:

$$P = \sigma\dot{\varepsilon} = G + J = \int_0^{\dot{\varepsilon}} \sigma \mathrm{d}\dot{\varepsilon} + \int_0^{\dot{\varepsilon}} \dot{\varepsilon} \mathrm{d}\sigma \tag{1}$$

where σ represents the flow stress (MPa) and $\dot{\varepsilon}$ is the strain rate (s^{-1}). The proportion of the dissipative power between G and J is determined by the m index, which is expressed as follows:

$$\frac{\partial J}{\partial G} = \frac{\partial \ln \sigma}{\partial \ln \dot{\varepsilon}} = m \tag{2}$$

Dissipation power J can be obtained with Equation (3) based on Equation (2).

$$J = \frac{m}{m+1}\sigma\dot{\varepsilon} \tag{3}$$

By comparing the J co-content with the maximum dissipation, J_{max}, the efficiency of power dissipation η of a non-linear dissipater is written as:

$$\eta = \frac{J}{J_{max}} = \frac{2m}{m+1} \tag{4}$$

A power-dissipation map can be constructed through the variation in dissipation coefficient with the temperature and strain rate. The η is an important parameter, indicating power dissipation and a higher η indicates a better processing condition. However, an unstable state, such as microcracks and shear bands, is also related to a high η value, thus the workability cannot be described completely. Prasad proposed the following instability criterion[19]:

$$\xi(\dot{\varepsilon}) = \frac{\partial \ln[m/(m+1)]}{\partial \ln \dot{\varepsilon}} + m < 0 \tag{5}$$

where ξ represents the dimensionless parameter. The variation in ξ with the deformation temperature and strain rate causes an instable region, characterized as $\xi < 0$. Finally, a processing map can be prepared by overprinting the power-dissipation map, containing stable and unstable regions.

2 EXPERIMENTAL PROCEDURES

The investigated material used in this project was the as-received Mg-13Gd-4Y-2Zn-0.5Zr (w/%) alloy, supplied by Yinguang Magnesium Industry Group Co., Ltd., and its chemical composition is shown in **Table 1**. It was pre-forged to eliminate defects and optimize the grain structure. Cylindrical specimens with a size of ϕ 8 mm × 12 mm were machined from the alloy. The initial microstructure of the specimens is shown in **Figure 1a**. It can be seen that the alloy was mainly composed of a Mg matrix, intragranular lamellar-shaped LPSO phases, interdendritic block-shaped LPSO phases and other eutectic phases. The average grain size was about 25 μm and the phase distribution was heterogeneous.

Uniaxial compression tests were carried out on a Gleeble-1500D thermo-mechanical simulator at strain rates in a range of 0.001–5 s^{-1} and deformation temperature range of 420–500 °C. The specimens were heated in a resistance furnace at a heating rate of 10 °C/s and kept at the target temperature for 180 s prior to isothermal compression. In order to reduce deformed friction, a graphite lubricant was used between a specimen and crosshead. After deformation, the specimen was immedi-

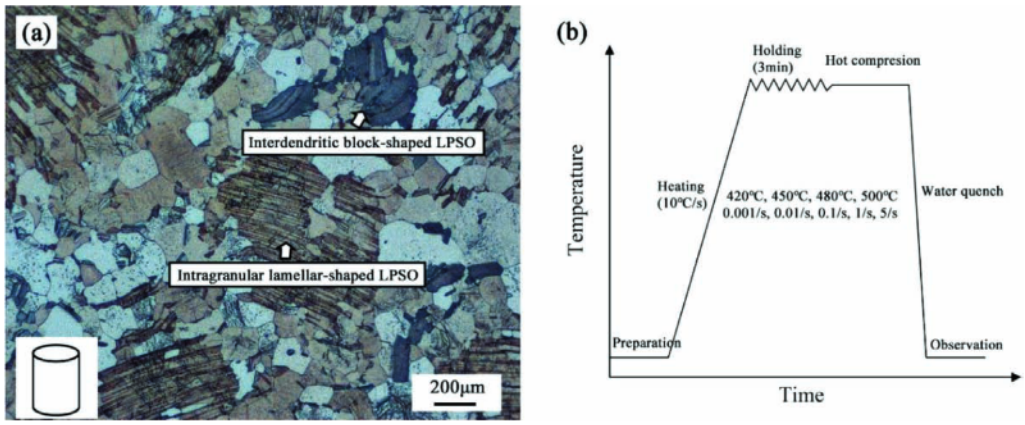

Figure 1: a) Microstructure of the as-received alloy, b) Schematic illustration of compression processing

ately quenched in water to maintain the deformed microstructure. We selected the observation surface that was parallel to the compression axis and ready for a metallographic examination using a Carl Zeiss optical microscope.

Table 1: Chemical composition of the tested alloy (*w*/%)

Element	Gd	Y	Zn	Zr	Fe	Ni	Mg
Content	12.8	4.0	1.8	0.42	≤0.001	≤0.002	Balanced

3 RESULTS AND DISCUSSION

3.1 Flow behavior

True stress/strain curves of the as-received Mg-13Gd-4Y-2Zn-0.5Zr alloy obtained in the temperature range of 420–500 °C and strain rates of 0.001–5 s^{-1} are shown in **Figure 2**. It can be seen that the alloy showed obvious dynamic-recrystallization characteristics, and the flow stress decreased with an increasing temperature and decreasing strain rate. The whole process can be approximately divided into three stages. Firstly, the flow stress went up sharply with an increasing strain due to work hardening. Secondly, the stress reached the peak σ_p, (which was the result of secondary strain hardening. The hardening rate in this stage was much lower than in the first one, and dynamic recovery (DRV) and DRX began to occur. As the strain continued to increase, the accumulation of dislocations induced DRX, and when DRX softening exceeded work hardening, the flow stress decreased. Finally, the interior of the material reached a relatively stable state and the curves were almost parallel.

The flow stress was an important factor, influencing the deformation process, and the forming mechanism could be clarified by studying the material's flow characteristics.[20] Based on further research of the curves, we now know the following facts:

(1) The Mg-13Gd-4Y-2Zn-0.5Zr alloy was more likely to reach a steady state at a high temperature and low strain rate. At a given temperature, the flow stress decreased with the decreasing strain rate. At a constant strain rate, the flow stress decreased with the increasing temperature. This was because the high temperature and low strain rate were conducive to dislocation slipping and annihilation, and the mobility of grain boundaries was also increased. In addition, DRX was easily induced at the elevated temperature and reduced strain rate, and DRX softening was sufficient to counterbalance the work-hardening effect. Meanwhile, the elevated temperature can result in a lower critical resolved shear stress (CRSS) for both basal and non-basal slip systems.

(2) The curves exhibited obvious serration at strain rates of 1 s^{-1} and 5 s^{-1}, and demonstrated multiple peaks. Jiang et al.[21] ascribed this to a fast grain-boundary-migration rate, and fast nucleation and growth of recrystallized grains at high strain rates.

(3) The deformation of Mg-13Gd-4Y-2Zn-0.5Zr was a thermal activation process, and DRX was the main mechanism.

3.2 Constitutive equation

Thermoplastic deformation is a process of thermal activation. To describe the relationship between the deformation temperature, strain rate and activation energy, a functional equation of the three parameters was estab-

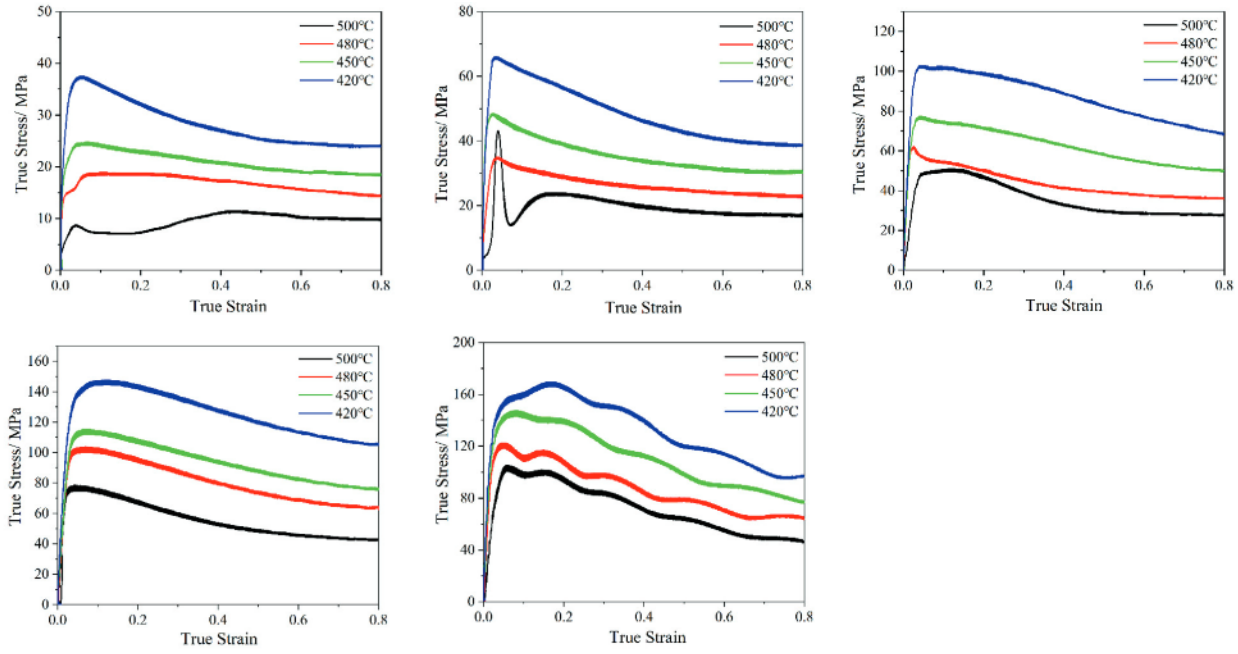

Figure 2: True stress/true strain curves of the specimens compressed at strain rates of: a) 0.001 s^{-1}, b) 0.01 s^{-1}, c) 0.1 s^{-1}, d) 1 s^{-1}, e) 5 s^{-1}

lished to predict the change in the rheological stress.[22] The commonly used phenomenological constitutive models include the Arrhenius, Johnson-Cook (J-C) and Zerilli-Armstrong (Z-A) models. The Z-A model is generally applied to face-centered cubic (FCC) or body-centered cubic (BCC) metals, but not to Mg alloys.[23] The J-A model is usually used in a constitutive analysis of metal deformation under high temperature and high strain rate, but rarely in the study of a thermal-deformation behavior at a low strain rate. Therefore, the Arrhenius equation was selected to model the deformation process of Mg-13Gd-4Y-2Zn-0.5Zr.

From the previous studies, we can conclude that the Zener-Hollomon (Z) parameter can depict the effects of deformation temperatures and strain rate on the flow-stress behavior. They can be expressed as follows:

$$\dot{\varepsilon} = A_1 \sigma^{n_1} \exp\left(-\frac{Q}{RT}\right) \quad (\alpha\sigma < 0.8) \tag{6}$$

$$\dot{\varepsilon} = A_2 \exp(\beta\sigma) \exp\left(-\frac{Q}{RT}\right) \quad (\alpha\sigma > 1.2) \tag{7}$$

$$\dot{\varepsilon} = A_2 [\sinh(\alpha\sigma)]^n \exp\left(-\frac{Q}{RT}\right) \tag{8}$$

$$Z = \dot{\varepsilon} \exp\left(\frac{Q}{RT}\right) = A[\sinh(\alpha\sigma)]^n \tag{9}$$

where Q is the activation energy (kJ/mol), R is the universal gas content (8.314 J/mol·K), and T is the absolute temperature (K). A_1, A_2, A, n_1, n, α and β are the material constants. Stress multiplier is defined as $\alpha = \beta/n$.

To simplify the equations, take the natural logarithms of both sides of Equations (6), (7), (8) and (9), and the equations are expressed as follows:

$$\ln \dot{\varepsilon} = \ln A_1 + n_1 \ln \sigma - \frac{Q}{RT} \tag{10}$$

$$\ln \dot{\varepsilon} = \ln A_2 + \beta\sigma - \frac{Q}{RT} \tag{11}$$

$$\ln \dot{\varepsilon} = \ln A + n \ln[\sinh(\alpha\sigma)] - \frac{Q}{RT} \tag{12}$$

$$\ln Z = \ln A + n \ln[\sinh(\alpha\sigma)] \tag{13}$$

The linear relationships of $\ln \sigma - \ln \dot{\varepsilon}$ and $\sigma - \ln \dot{\varepsilon}$ at different temperatures are shown in **Figures 3a** and **3b**. According to Equations (10) and (11), the values of $1/n_1$ and $1/\beta$ can be derived from the slopes of $\ln \sigma - \ln \dot{\varepsilon}$ and $\sigma - \ln \dot{\varepsilon}$. Hence, the average values of n_1 and β were found to be 4.79323924 and 0.07690867 MPa^{-1}, respectively. The mean value of α was 0.01604524 MPa^{-1} according to $\alpha = \beta/n$.

Taking the logarithms of both sides of Equation (12), we get the expression of deformation activation energy Q:

$$Q = R\left\{\frac{\partial \ln \dot{\varepsilon}}{\partial \ln[\sinh(\alpha\sigma)]}\right\}_T \left\{\frac{\partial \ln[\sinh(\alpha\sigma)]}{\partial(1/T)}\right\}_{\dot{\varepsilon}} \tag{14}$$

$\left\{\frac{\partial \ln \dot{\varepsilon}}{\partial \ln[\sinh(\alpha\sigma)]}\right\}_T$ is the slope of the fitting relation of $\ln(\sinh(\alpha\sigma)) - \ln \dot{\varepsilon}$ at different temperatures, as

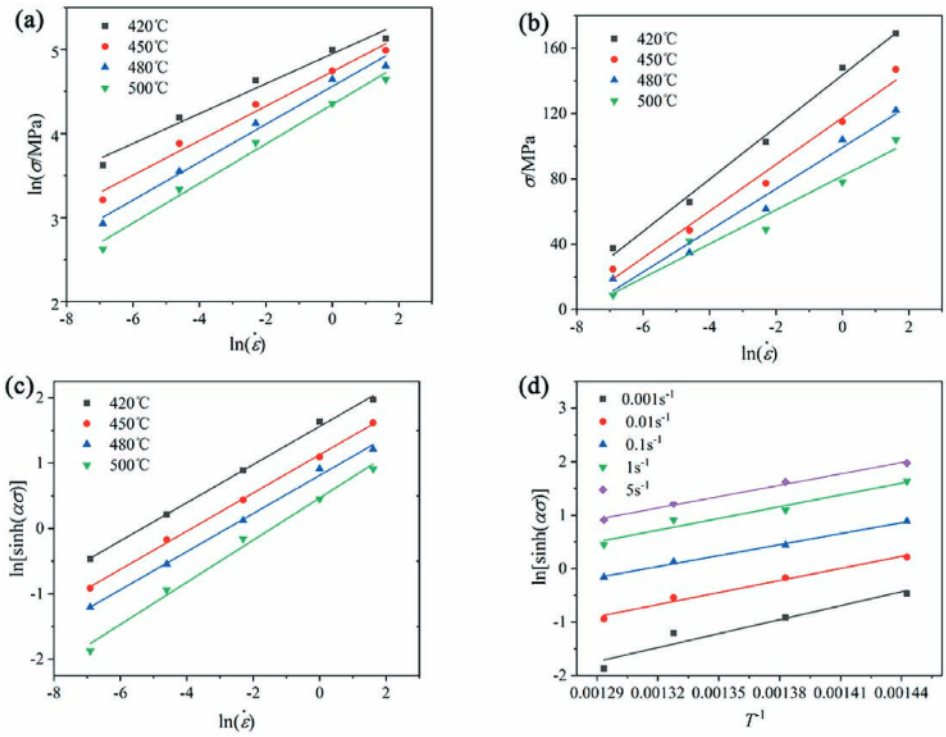

Figure 3: Relationships of: a) $\ln \sigma - \ln \dot{\varepsilon}$, b) $\sigma - ln\ \dot{\varepsilon}$, c) $\ln(\sinh(\alpha\sigma)) - \ln \dot{\varepsilon}$, d) $\ln(\sinh(\alpha\sigma)) - T^{-1}$

shown in **Figure 3c**. $\left\{\frac{\partial \ln[\sinh(\alpha\sigma)]}{\partial(1/T)}\right\}_{\dot{\varepsilon}}$ is the slope of ln (sinh($\alpha\sigma$)) – T^{-1}, as demonstrated in **Figure 3d**.

Putting the average slope of ln (sinh($\alpha\sigma$)) – ln $\dot{\varepsilon}$ and ln (sinh($\alpha\sigma$)) – T^{-1} into Equation (14), we find that the average Q value of the as-received Mg-13Gd-4Y-2Zn-0.5Zr alloy is 208.224 kJ/mol.

Plastic deformation is a process of thermal activation, in which atoms move rapidly. When atoms reach the required energy, deformation takes place. Therefore, the value of Q is an important parameter when determining a deformation difficulty. It can be influenced by material characteristics, deformation parameters, dynamic precipitation, dislocation pinning and secondary phases.[24] Table 2 lists the Q values of pure Mg and some Mg alloys. It can be seen that the activation energy of pure Mg is 135 kJ/mol, while the Q values for most of Mg alloys are higher than that of pure Mg. Furthermore, additions of Gd and Y to Mg alloys can effectively increase the activation energy, owing to the enhanced solution strengthening, precipitation strengthening and the formation of secondary phases, hindering the dislocation slipping. In the present research, the Q of the Mg-13Gd-4Y-2Zn-0.5Zr alloy was 208.2 kJ/mol, which was higher than for the traditional Mg alloys. The existence of the LPSO phase strengthened the Mg matrix and hindered the slip of dislocations.[14] Thus, a Mg alloy containing rare-earth elements is a kind of a hard-to-deform metal.

Table 2: Comparison between pure Mg and other Mg alloys

Material	Activation energy (kJ/mol)	References
Pure Mg	135	[25]
Mg-3Al-Zn	132.4	[26]
Mg-9Al-Zn	136.3	[27]
Mg-9.5Zn-2Y	176.3	[28]
Mg-9Gd-2.4Y-0.4Zr	199.8	[27]
Mg-13Gd-4Y-2Zn-0.5Zr	208.2	This study

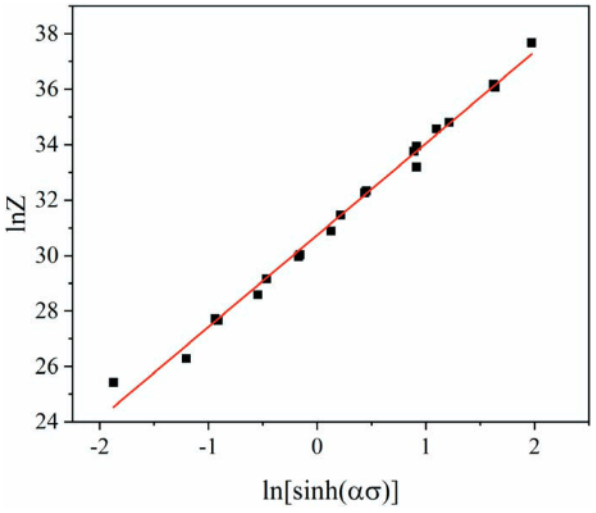

Figure 4: Relationship between the Z parameter and peak stress

The Zener-Hollomon (Z) parameter was important for measuring the effect of the deformation temperature and strain rate on the thermal-deformation behavior. **Figure 4** shows the linear fitting relationship between the Z parameter and peak stress based on the least-square method. The functional relationship between ln Z and ln (sinh ($\alpha\sigma$)) was obtained with Equation (13). In accordance with the slope and intercept of the linear fitting curve, we found that ln A = 30.73574 and n = 3.30991.

$$\ln Z = 30.73574 + 3.30991 \ln[\sinh(\alpha\sigma)] \quad (15)$$

The value of A was 2.2303×10^{13}. Putting n, α, Q and A into Equation (8), the following constitutive equation of the as-received Mg-13Gd-4Y-2Zn-0.5Zr alloy can be obtained:

$$\dot{\varepsilon} = 2.2303\times10^{13}\left[\sinh(0.01604524\sigma)\right]^{4.79323924} \times \times \exp\left(-\frac{208.2}{8.314T}\right) \quad (16)$$

3.3 Processing maps and microstructure evolution

Based on the thermal simulation deformation, a DMM was constructed to describe the relationships between deformation parameters, microstructure and processing properties. The processing map was an important mean to understand the material deformation law and optimize the processing conditions, especially for the hard-to-deform Mg-RE-Zn alloy.

The processing maps of the Mg-13Gd-4Y-2Zn-0.5Zr alloy, developed at strains of 0.3, 0.5 and 0.7 are shown in **Figure 5**, where the x-axis is the deformation temperature, y-axis is the strain rate, z-axis represents the dissipation rate and the contour line represents the power-dissipation factor. In the contour processing maps, the gray regions are flow-instability areas, while the others are flow-stability areas. In the three-dimensional processing maps, red regions indicate high efficiency of power dissipation, while others indicate low efficiency of power dissipation.

It can be seen from **Figure 5** that, according to the processing maps, the change in the strain (increasing from 0.3 to 0.7) has a limited effect on plastic deformation. High power-dissipation domains were mainly located in the regions of high temperature and low strain rate, which was due to the increased dislocation slipping ability with the increasing deformation temperature and enhanced dynamic-recrystallization process due to an increase in the energy storage. Meanwhile, the low stain rate improved the grain-boundary migration, which was beneficial to the dislocation annihilation. When the strain reached 0.3, as shown in **Figures 5a** and **5b**, the maximum power-dissipation coefficient was 0.36–0.40, which occurred in a temperature range of 480–500 °C and at a stain rate of 0.001 s^{-1}. At the strain of 0.5, shown in **Figures 5c** and **5d**, the maximum power dissipation was almost the same as with the strain of 0.3, and an optimum

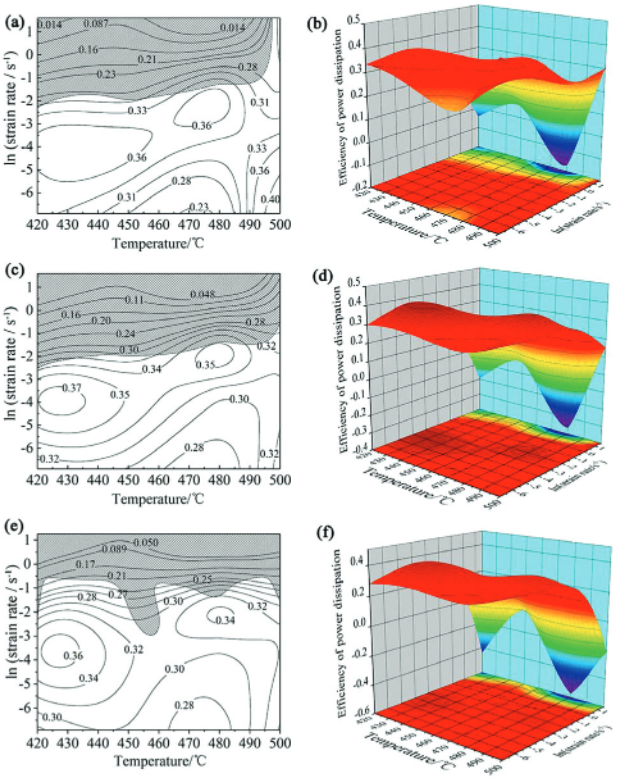

Figure 5: Processing maps of Mg-13Gd-4Y-2Zn-0.5Zr alloy: a and b) strain of 0.3, c and d) strain of 0.5, e and f) strain of 0.7

deformation-temperature range of 420–445 °C and a strain rate of 0.01 s^{-1} were observed. When the strain increased to 0.7, as shown in **Figures 5c** and **5d**, a peak efficiency coefficient of about 0.34–0.36 was obtained in a temperature range of 420–445 °C and at the strain rate of 0.01 s^{-1}.

Wang et al.[29] found that the obvious changes in the power dissipation, temperature and strain rate may be related to the effect of the LPSO-phase evolution. In addition, when observing the flow-instability domains, it can be noticed that the high stain rate at both high and low deformation temperatures can lead to a deformation failure. From the analysis of the Mg-alloy characteristics and deformation mechanism, it is clear that the HCP structure and low deformation temperature hindered the activation of the slip system. Meanwhile, the deformation resistance of the Mg alloy was increased and the DRX process was inhibited. The activation energy of thermal deformation was improved with the increasing temperature, while the ability of dislocation slipping and climbing was also increased, which led to the occurrence of DRV and DRX.[30] However, a serious dislocation accumulation took place in the grains in the case of a high strain rate so that the flow instability occurred easily, causing failures such as cracks.

Figure 6 shows the typical microstructure of the Mg-Gd-Y-Zn-Zr alloy deformed at different temperatures at the same strain rate of 0.01 s^{-1}. It can be seen that the deformation temperature exerted remarkable influences on the microstructure after compression. The alloy deformed at 420 °C exhibited a relatively fine equiaxed-grain structure with block-shaped LPSO phases, which suggested that DRX occurred during hot deformation. According to **Figure 6a**, parts of grains and LPSO phases were obviously elongated, and the grains had zigzag boundaries. The main softening mechanism was DRX, but it was not completely finished according to the heterogeneous grain structure. The grain size of the Mg-Gd-Y-Zn-Zr alloy deformed at 450 °C was larger than that at 420 °C, which can be attributed to the diffusion abilities of atoms at higher temperatures, cross-slip of dislocation and enhanced migration of grain boundaries. Meanwhile, all these conditions were beneficial to the growth of DRX, as shown in **Figure 6b**. At a deformation temperature of 480 °C, the grain size was further increased, but the area of the fraction of block-shaped LPSO phases was decreased, which may be attributed to the solid solution at high temperature.

Optical micrographs of the Mg-Gd-Y-Zn-Zr alloy deformed at different strain rates at a given temperature of 450 °C are shown in **Figure 7**. It can be noticed that the strain rate can obviously influence the microstructure evolution at a given deformation temperature. At the relatively low strain rate of 0.001 s^{-1}, the structure was composed of heterogeneous grains and large LPSO phases. This was due to the dislocations that were reorganized through climbing and sliding, which led to a slight decrease of the dislocation intensity. Meanwhile, the DRX fine grains trapped the dislocations and released the stress concentration, resulting in a growth of

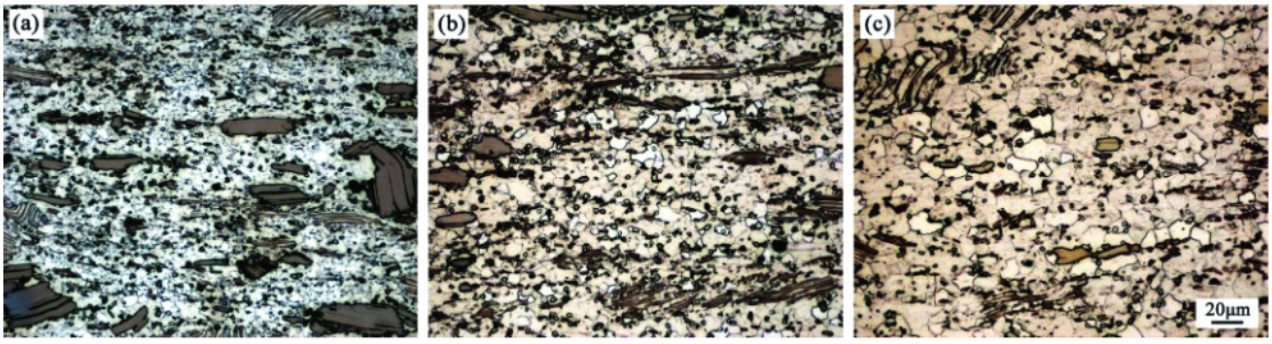

Figure 6: Microstructures of the test alloy with strain rate of 0.01 s^{-1} and compressed at: a) 420 °C, b) 450 °C, c) 480 °C

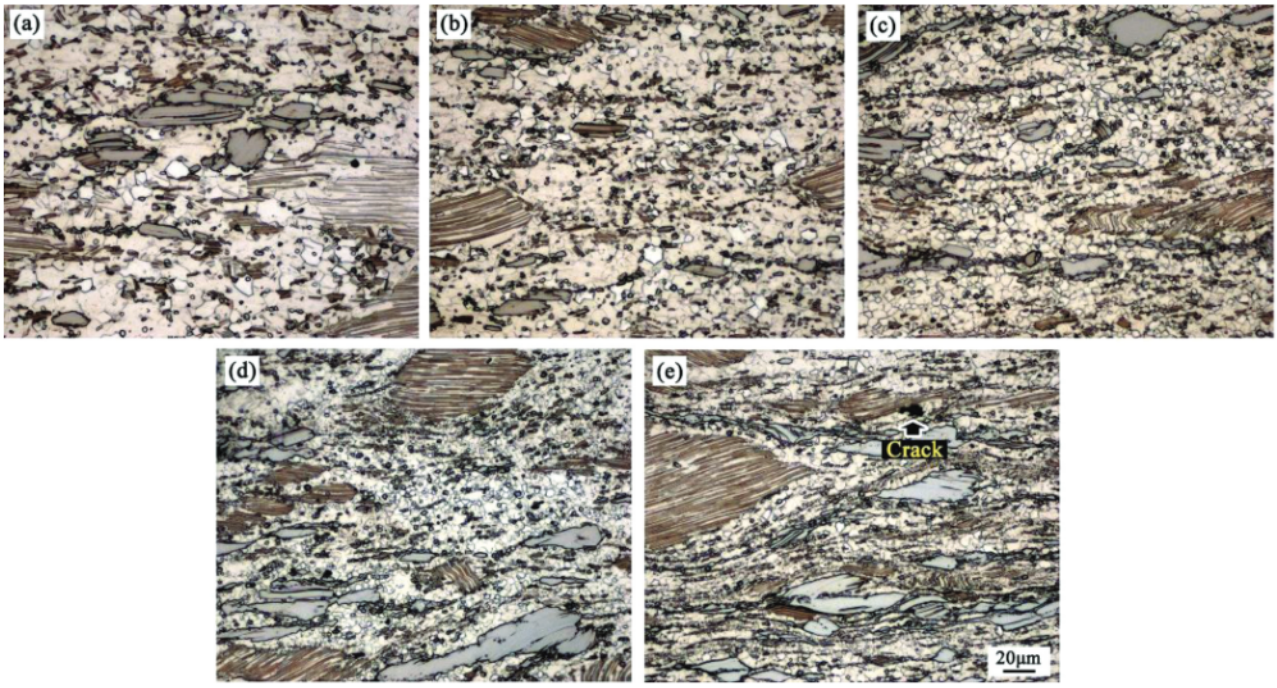

Figure 7: Microstructures of the Mg-Gd-Y-Zn-Zr alloy tested at the temperature of 450 °C and the strain rates: a) 0001 s^{-1}, b) 0.01 s^{-1}, c) 0.1 s^{-1}, d) 1 s^{-1}, e) 5 s^{-1}

fine grains. With the strain rate increasing to 0.01 s^{-1} and 0.1 s^{-1}, as shown in **Figures 7b** and **7c**, the DRX fine grains and broken LPSO phases were clearly observed. It can be easily found from the rheological structure that there were large amounts of dislocations at the higher strain rates of 1 s^{-1} and 5 s^{-1}, as shown in **Figures 7d** and **7e**. Meanwhile, shear bands and cracks can be seen in the specimens deformed at 5 s^{-1}, which can be attributed to the stress concentration. Local stress can be concentrated at the interfaces between grain boundaries and LPSO phases during compression, causing dislocation piling up and rearrangement and, in turn, forming sub-grains.[31] With further deformation, DRX grains can be observed due to the change in the sub-grains from low angle boundaries to high angle grain boundaries. Thus, the main dynamic softening mechanisms were DRV and DRX during the hot-compression tests.

In conclusion, the deformation temperature and strain rate had a remarkable effect on the microstructure evolution. DRX was a beneficial process during hot compression since it can provide a stable flow behavior and ideal workability of the material by simultaneously softening and reconstituting the microstructure. Due to this, on the basis of the processing maps and microstructural evolution, there were two optimum processing domains of the Mg-Gd-Y-Zn-Zr alloy: one occurred in the strain-rate range of 0.01–0.05 s^{-1} and deformation-temperature range of 420–445 °C, the other occurred at the strain-rate range of 0.05–0.1 s^{-1} and deformation-temperature range of 475–490 °C.

4 CONCLUSIONS

In the present research, the hot-deformation behavior of the as-received Mg-Gd-Y-Zn-Zr alloy achieved via hot compression tests was investigated in a deformation temperature range of 420–500 °C and strain-rate range of 0.001–5 s^{-1}. The conclusions drawn from the study are as follows:

1. The flow stress and deformed microstructure strongly depended on the deformation temperature and strain rate. The flow stress increased with the increasing strain rate and decreasing compression temperature. DRV and DRX were the main softening mechanisms, and the growth of DRX grains was observed at a relatively high temperature and low strain rate. Shear bands and cracks occurred in the Mg-Gd-Y-Zn-Zr alloy deformed at the strain rate of 5 s^{-1}.

2. A constitutive equation for the Mg-Gd-Y-Zn-Zr alloy was established using a hyperbolic-sine-type equation to describe the strain-rate and compression-temperature dependence of the flow stress, which was $\dot{\varepsilon} = 2.2303 \times 10^{13} \left[\sinh(0.01604524\sigma)\right]^{4.79323924} \times$ $\times \exp(-208.2/8.314T)$. Deformation activation energy Q was 208.2 kJ/mol.

3. Based on a DMM, processing maps for strains of 0.3, 0.5 and 0.7 were generated. It can be concluded from power-dissipation maps that the instability domain was mainly concentrated at low temperature and high strain rate, and a change in the strain had little effect on it. The optimum processing domains were located at temperatures of 420–445 °C and strain rates of 0.01–0.05 s^{-1},

and temperatures of 475–490 °C and strain rates of 0.05–0.1 s^{-1}.

Acknowledgment

This study was supported by the National Science Foundation of China under Grant nos. 51775520 and 52075501.

5 REFERENCES

[1] J. Zhang, S. Liu, R. Wu, L. Hou, M. Zhang, Recent developments in high-strength Mg-RE-based alloys: Focusing on Mg-Gd and Mg-Y systems, J. Magnes. Alloy, 6 (**2018**) 3, 277–291, doi:10.1016/j.jma.2018.08.001

[2] Z. Yan, X. Li, J. Zheng, Z. Zhang, Q. Wang, K. Xu, H. Fan, G. Zhang, J. Zhu, Y. Xue, Microstructure evolution, texture and mechanical properties of a Mg-Gd-Y-Zn-Zr alloy fabricated by cyclic expansion extrusion with an asymmetrical extrusion cavity: The influence of passes and processing route, J. Magnes. Alloys, 9 (**2021**) 3, 964–982, doi:10.1016/j.jma.2020.06.016

[3] L. Song, Y. Zhang, Y. Lu, X. Li, J. Wang, J. Wang, Microstructure, texture and mechanical properties of a friction-stir-processed Mg-Al-Ca-Mn-Zn alloy, Mater. Tehnol., 53 (**2019**) 6, 839–844, doi:10.17222/mit.2019.090

[4] G. Wu, C. Wang, M. Sun, W. Ding, Recent developments and applications on high-performance cast magnesium rare-earth alloys, J. Magnes. Alloys, 9 (**2021**) 1, 1–20, doi:10.1016/j.jma.2020.06.021

[5] W. Wang, Y. Qiu, J. Jia, X. Yan, W. Zhang, Influence of samarium on the microstructure and mechanical properties of Mg-Y-Zn-Zr alloys, Mater. Tehnol., 52 (**2018**) 4, 405–410, doi:10.17222/mit.2017.175

[6] Z. Yan, Z. Zhang, X. Li, J. Xu, Q. Wang, G. Zhang, J. Zheng, H. Fan, K. Xu, J. Zhu, Y. Xue, A novel severe plastic deformation method and its effect on microstructure, texture and mechanical properties of Mg-Gd-Y-Zn-Zr alloy, J. Alloy. Compd., 822 (**2020**) 153698, doi:10.1016/j.jallcom.2020.153698

[7] B. Liu, F. Liu, N. Yang, X. Zhai, L. Zhang, Y. Yang, B. Li, J. Li, E. Ma, J. Nie, Z. Shan, Large plasticity in magnesium mediated by pyramidal dislocations, Science, 365 (**2019**) 6448, 73–75, doi:10.1126/science.aaw2843

[8] T. Homma, N. Kunito, S. Kamado, Fabrication of extraordinary high-strength magnesium alloy by hot extrusion, Scripta Mater., 61 (**2009**) 6, 644–647, doi:10.1016/j.scriptamat.2009.06.003

[9] N. Ogawa, M. Shiomi, K. Osakada, Forming limit of magnesium alloy at elevated temperatures for precision forging, Inter. Mach. Tool. Manu., 42 (**2002**), 607–614, doi:10.1016/s0890-6955(01)00149-3

[10] A. R. Eivani, S. M. Mirghasemi, S. H. Seyedein, J. Zhou, H. R. Jafarian, Simulation of deformation and fracture initiation during equal channel angular pressing of AZ31 magnesium alloy with covered tube casing, J. Mater. Res. Technol., 12 (**2021**), 1913–1923, doi:10.1016/j.jmrt.2021.03.096

[11] B. Li, B. Teng, G. Chen, Microstructure evolution and mechanical properties of Mg-Gd-Y-Zn-Zr alloy during equal channel angular pressing, Mater. Sci. Eng. A, 744 (**2019**), 396–405, doi:10.1016/j.msea.2018.12.024

[12] B. Li, Q. Pan, Z. Yin, Characterization of hot deformation behavior of as-homogenized Al-Cu-Li-Sc-Zr alloy using processing maps, Mater. Sci. Eng. A, 614 (**2014**), 199–206, doi:10.1016/j.msea.2014.07.031

[13] N. Srinivasan, Y. V. R. K. Prasad, P. Rama Rao, Hot deformation behaviour of Mg-3Al alloy – A study using processing map, Mater. Sci. Eng. A, 476 (**2008**) 1–2, 146–156, doi:10.1016/j.msea.2007.04.103

[14] X. Zhou, C. Liu, Y. Gao, S. Jiang, W. Liu, L. Lu, Hot compression behavior of the Mg-Gd-Y-Zn-Zr alloy filled with intragranular long-period stacking ordered phases, J. Alloy. Compd., 724 (**2017**), 528–536, doi:10.1016/j.jallcom.2017.07.088

[15] Z. Zhang, Q. Huo, Z. Xiao, A. Hashimoto, X. Yang, Microstructural evolutions and mechanical properties of Mg-xY-2Nd-0.2Zn-0.5Zr (x=0, 2, 4, 6 and 8) alloy under hot compression, Mater. Sci. Eng. A, 722 (**2020**), 138816, doi:10.1016/j.msea.2019.138816

[16] X. Xia, Q. Chen, J. Li, D. Shu, C. Hu, S. Huang, Z. Zhao, Characterization of hot deformation behavior of as-extruded Mg-Gd-Y-Zn-Zr alloy, J. Alloy. Compd., 610 (**2014**), 203–211, doi:10.1016/j.jallcom.2014.04.210

[17] X. Zhou, Y. Yao, J. Zhang, X. Chen, W. Huang, J. Pan, H. Wang, M. Weng, A high-performance Mg-4.9Gd-3.2Y-1.1Zn-0.5Zr alloy via multidirectional forging after analyzing its compression behavior, J. Mater. Sci. Technol., 70 (**2021**), 156–167, doi:10.1016/j.jmst.2020.08.054

[18] Y. V. R. K. Prasad, S. Sasidhara, Hot Working Guide: A Compendium of Processing Maps, ASM International, Materials Park, OH, 1997

[19] Y. V. R. K. Prasad, T. Seshacharyulu, Processing maps for hot working of titanium alloys, Mater. Sci. Eng. A, 243 (**1998**) 1–2, 82–88, doi:10.1016/S0921-5093(97)00782-X

[20] B. Li, B. Teng, W. Xu, Hot deformation characterization of homogenized Mg-Gd-Y-Zn-Zr alloy during isothermal compression, JOM, 71 (**2019**) 11, 4059–4070, doi:/10.1007/s11837-019-03556-y

[21] S. Jiang, C. Liu, H. Li, X. Zhang, Dynamic recrystallization of high purity polycrystalline aluminum, J. Cen. South. Univ., 35 (**2004**) 6, 935–940

[22] R. Alizadeh, R. Mahmudi, O. A. Ruano, A. H. W. Ngan, Constitutive analysis and hot deformation behavior of fine-grained Mg-Gd-Y-Zr alloys, Metall. Mater. Trans. A, 48A (**2017**) 11, 5699–5709, doi:10.1007/s11661-017-4311-7

[23] Z. Zhang, Z. Yan, Y. Du, G. Zhang, J. Zhu, L. Ren, Y. Wang, Hot deformation behavior of homogenized Mg-13.5Gd-3.2Y-2.3Zn-0.5Zr alloy via hot compression tests, Materials, 11 (**2018**) 11, 2282, doi:10.3390/ma11112282

[24] H. Miura, M. Ito, X. Yang, J. J. Jonas, Mechanisms of grain refinement in Mg-6Al-1Zn alloy during hot deformation, Mater. Sci. Eng. A, 538 (**2012**), 63–68, doi:10.1016/j.msea.2012.01.014

[25] H. J. Frost, M. F. Ashby, Deformation mechanism maps, the plasticity and creep of metals and ceramics, Pergamon Press, London 1982

[26] Q. Wang, J. Lin, Q. Huang, C. Wang, The flow stress during hot deformation of AZ31 magnesium alloy, J. Taiyuan Univ. Sci. Technol., 35 (**2014**) 4, 274–279

[27] H. Mirzadeh, Quantification of the strengthening effect of rare earth elements during hot deformation of Mg-Gd-Y-Zr magnesium alloy, J. Mater. Res. Technol., 5 (**2016**) 1, 1–4, doi:10.1016/j.jmrt.2015.03.001

[28] T. Y. Kwak, H. K. Lim, W. J. Kim, Hot compression characteristics and processing maps of a cast Mg-9.5Zn-2.0Y alloy with icosahedral quasicrystalline phase, J. Alloy. Compd., 644 (**2015**), 645–653, doi:10.1016/j.jallcom.2015.04.158

[29] C. Wang, Y. Liu, T. Lin, T. J. Luo, Y. H. Zhao, H. Hou, Y. S. Yang, Hot compression deformation behavior of Mg-5Zn-3.5Sn-1Mn-0.5Ca-0.5Cu alloy, Mater. Charact., 157 (**2019**), 109596, doi:10.1016/j.matchar.2019.109896

[30] L. Zhu, Q. Li, X. Chen, Q. Zhang, Effect of Sm on dynamic recrystallization of Mg-8Gd-0.5Zr alloy during hot compression, J. Alloy. Compd., 865 (**2021**), 158648, doi:10.1016/j.jallcom.2021.158648

[31] X. Xia, K. Zhang, X. Li, M. Ma, Y. Li, Microstructure and texture of coarse-grained Mg-Gd-Y-Nd-Zr alloy after hot compression, Mater. Des., 44 (**2013**), 521–527, doi:10.1016/j.matdes.2012.08.043